MS 5348 - Revision 1

Aluminum environments in synthetic Ca-Tschermak clinopyroxene ($CaAlAlSiO_6$) from Rietveld refinement, ^{27}Al NMR and first-principles calculations.

Roberta L. Flemming[1]*, Victor Terskikh[2] and Eric Ye[2]

1. Department of Earth Sciences, Western University, London, Ontario N6A 5B7, Canada
2. Department of Chemistry, University of Ottawa, Ottawa, Ontario, K1N 6N5, Canada

* E-mail of corresponding author: rflemmin@uwo.ca

ABSTRACT

^{27}Al magic-angle spinning nuclear magnetic resonance (MAS NMR) and ^{27}Al triple quantum (3Q) MAS NMR spectroscopy have been performed at 21.1 Tesla (T), as a direct probe of environment around Al in synthetic Ca-Tschermak's clinopyroxene, $CaAlAlSiO_6$, henceforward referred to as CaTs. For comparison, ^{27}Al MAS NMR of CaTs has also been performed at 14.1 T. The ^{27}Al 3QMAS NMR spectrum of CaTs has revealed a variety of local environments around octahedral and tetrahedral Al, both ordered and disordered, symmetrical and distorted. Rietveld refinement of powder X-ray diffraction data has confirmed the high-temperature, long-range disordered C2/c structure for this sample.

The ^{27}Al MAS NMR spectra of CaTs look broadly similar at 14.1 and 21.1 T. Both spectra exhibit two distinct peaks at the octahedral site and an irregularly-shaped, broad tetrahedral site. The line widths are significantly broader at lower field and the ^{27}Al 3QMAS NMR spectrum at 21.1 T exhibits several additional peaks: At least three peaks were resolved at the octahedral site (in both the MAS spectrum along F2 and the 3Q spectrum along F1), whereas two peaks are clearly resolved at the tetrahedral site at 21.1 T. One tetrahedral peak, observed at both fields, is broad in F1 and narrow in F2, spread along the isotropic shift diagonal, indicating a highly disordered but relatively symmetric environment. The second peak, newly-observed at 21.1 T, is narrow in F1 but very broad in F2, indicating an ordered but highly-distorted environment. This peak has not been observed at lower magnetic field strengths.

Octahedral peak assignments have been made according to the number of Al atoms in the six tetrahedral sites around M1, where an increasing number of NNN

tetrahedral Al (2Al, 3Al and 4Al) is correlated with displacement of the chemical shift to higher frequency. Assigned sites are similar to the local tetrahedral environments around M1 in ordered $P2_1/n$ or C2 structures, suggesting the presence of ordered domains in this otherwise disordered C2/c structure. To aid in the interpretation of these tetrahedral Al environments, Density Functional Theory (DFT) calculations have been performed using two approximations of the CaTs crystal structure: fully ordered tetrahedral chains or fully disordered tetrahedral chains. These calculations suggest that the tetrahedral Al site is a sensitive indicator of order-disorder in CaTs. Tetrahedral Al sites in ordered tetrahedral chains (Si-O-Al-O-Si…) are predicted to have only large C_Q whereas tetrahedral Al sites in disordered systems (Al-O-Al-O-Al…) are predicted to have only small C_Q. Both environments appear to exist in the synthetic CaTs sample in this study. Cation order-disorder has implications for thermobarometry based on CaTs-containing pyroxenes.

The discovery of the new highly-distorted tetrahedral site at ultrahigh magnetic field suggests that highly-distorted Al sites in silicate minerals may be NMR-invisible in ^{27}Al 3QMAS NMR spectra acquired at lower fields, and these will have been systematically overlooked. This underscores the necessity to collect ^{27}Al NMR spectra of silicates at the highest available magnetic field strength.

Keywords: CaTs, 3QMAS NMR, Density Functional Theory, Si-Al order-disorder, site distortion, aluminous pyroxene, single chain silicate, Rietveld refinement, VOLCAL

INTRODUCTION

Pyroxenes are major constituents of the Earth's crust and upper mantle to depths of 400 km, and are potentially important indicators of the temperature and pressure

conditions of their formation. Aluminous pyroxenes, including end-members jadeite ($NaAlSi_2O_6$) and Ca-Tschermak pyroxene (CaTs: $CaAl_2SiO_6$), undergo solid solution with diopside ($CaMgSi_2O_6$), producing omphacite, $(Na,Ca)[Mg,Al]Si_2O_6$, and aluminous diopside, $Ca[Mg,Al](Al,Si)O_6$, also known colloquially as 'fassaite', respectively.

Although omphacite is more commonly encountered than aluminous diopside (fassaite) on Earth, aluminous diopside (fassaite) is more common across the solar system, where it is found in several planetary bodies. First identified structurally in the Allende CV3 carbonaceous chondrites (Dowty and Clark 1973), it has been studied in many carbonaceous chondrites (e.g. Ma et al. 2009) as a major component of Calcium Aluminum-rich Inclusions (CAIs); these are high-temperature refractory materials which formed as early solids in the solar nebula (see for example Brearley and Jones 1998). Aluminous diopside (fassaite) is also known to be a major phase in the Angrite meteorites (Hazen and Finger 1977; Mittlefehldt et al. 2002).

CaTs-rich pyroxenes are found in mafic rocks (Dal Negro et al. 1986; Kogiso et al. 2004), silica undersaturated rocks (Dal Negro et al. 1985), lamprophyric alnöites (Durazzo 1999), carbonatites (Pecor 1967), and skarns (Pascal 2005); CaTs is an important component of pyroxene formed from magma-carbonate interaction (Gaeta et al. 2009; Mollo et al. 2010). In a meteoritics context, end-member CaTs ($CaAlAlSiO_6$) has been recently renamed kushiroite (Kimura et al. 2009), but in this work on a synthetic sample we retain the CaTs terminology.

Omphacite and CaTs solid solutions have been used as important components in geobarometers (e.g., Putirka et al. 1996; Nimis and Ulmer 1998; Yoshino et al. 1998; Nimis 1995; 1999; Ashchepkov 2002; Etzel et al. 2007; Putirka 2008). Omphacite is

indicative of high pressures and a range of temperatures whereas CaTs is indicative of high temperatures and moderate pressures (Deer et al. 1978). A complication that arises in attempting to apply aluminous pyroxene geobarometers is the potential for cation order-disorder on both sublattices, through Tschermak's substitution of Al simultaneously into both the tetrahedral and octahedral sites (denoted ( ) and [ ], respectively), according to $(Si^{4+}) + [Mg^{2+}] = (Al^{3+}) + [Al^{3+}]$. The substitution will modify the configurational entropy and enthalpy of the pyroxene, leading to displacements in the location of phase boundaries involving CaTs pyroxene. There is, however, a paucity of measurements for Si-Al order-disorder on the tetrahedral sites and Mg-Al order-disorder on the octahedral sites. This work examines the structure and Si-Al ordering in end-member CaTs using Rietveld refinement of powder diffraction data and ^{27}Al NMR spectroscopy, as well as quantum chemical computations using Density Functional Theory (DFT).

CaTs theory and experimental design

At high temperatures, CaTs has space group C2/c (Figure 1), implying complete Si-Al disorder on the single chain; but at low temperatures, long-range ordering in the structure is expected to induce a phase transition from C2/c to lower symmetry. For example, Okamura et al. (1974) proposed four possible ordered Si-Al tetrahedral arrangements for end-member CaTs, having symmetries C2, C-1, P2/n and $P2_1/n$. Cohen (1986) predicted the most energetically favorable ordering transition in CaTs to be from C2/c to $P2_1/n$, using a pair approximation model. Bosenick et al. (2001) similarly predicted a transition from C2/c to $P2_1/n$ from Monte Carlo simulations. They noted that

it would occur below 727 °C, which is well below the stability field of CaTs relative to grossular and corundum (Hays 1966; Wood and Holloway 1984). Although long-range ordering has not been observed in CaTs, short-range ordered domains are suggested to exist above the transition temperature (Grove and Burnham 1974). X-ray methods cannot distinguish Si and Al on the tetrahedral site due to their similar scattering behavior; Al-Si cation ordering must be indirectly inferred from bond length variation. Short-range ordered domains would, however, be directly observable by nuclear magnetic resonance (NMR) spectroscopy.

Magic angle spinning nuclear magnetic resonance spectroscopy (MAS NMR) has previously been used to examine cation ordering in aluminous pyroxenes (Millard and Luth 1998). In the diopside ($CaMgSi_2O_6$) - CaTs ($CaAl_2SiO_6$) solid solution, extensive Si-Al ordering on the tetrahedral chain has been observed directly using ^{29}Si MAS NMR (Millard and Luth 1998: Flemming and Luth 2002). ^{29}Si MAS NMR of these chain silicates was also found to be sensitive to Al substitution at the octahedral site, thus enabling indirect observation of the octahedral environment. Building here on these previous Si-based studies, ^{27}Al MAS NMR can provide direct observation of both the octahedral and tetrahedral sites. Furthermore, ^{27}Al is a quadrupolar nucleus (I=5/2) and as such it can give additional information about site distortion through interaction of its electric quadrupole moment (eQ) with the electric field gradient (EFG = V_{zz}). For non-spherical cation sites ($V_{zz} > 0$) in minerals, the electric quadrupolar interaction produces quadrupolar broadening and distinctive quadupolar lineshapes. The quadrupolar interaction is defined by the quadrupole coupling constant (C_Q) according to equation 1 (e.g. Kirkpatrick 1988).

$$C_Q = eQV_{ZZ} / h \quad \ldots\ldots 1.$$

The size of C_Q is related to the deviation of the site asymmetry tensor from spherical ($V_{ZZ} = 0$). The distribution of the EFG tensor is defined by the asymmetry parameter (η) according to equation 2 (e.g. Kirkpatrick 1988):

$$\eta = | V_{XX} - V_{YY} | / V_{ZZ} \quad \ldots\ldots 2.$$

where $\eta = 0$ for axially symmetric site symmetry while $\eta = 1$ for a non-symmetric site. Thus, quadrupolar nuclei reveal useful information about Al site symmetry and distortion.

The technique of multiple quantum (MQ) MAS NMR (Frydman and Harwood 1995: Rocha et al. 2005) has been found to give very highly resolved ^{27}Al NMR spectra for a variety of Earth materials (e.g. Baltisberger et al. 1996; Alemany et al. 1999, 2000; Ashbrook et al. 2000; Hawthorne et al. 2000; Sani et al. 2001; Damodaran et al. 2002; Gore et al. 2002; Xue and Kanzaki 2008; Florian et al. 2012) via additional resolution within the octahedral and tetrahedral regions of the NMR spectrum.

Furthermore, Density Functional Theory (DFT) provides a useful predictive tool to assist in the interpretation of NMR chemical shifts and quadrupolar parameters by generating predicted NMR parameters (see Bonhomme et al. 2012). This technique is useful for glasses (e.g. Pedone et al. 2010, 2012; Gambuzzi et al. 2014) and crystalline materials (e.g. Choi et al. 2009; Ferrara et al. 2013). DFT modeling relies on crystal structural information, such as can be determined by Rietveld refinement of powder X-ray diffraction data for example (e.g. Ferrara et al. 2013; Biswal et al. 2012). This integrated experimental-computational approach improves our predictive capability by

linking crystal structural parameters to solid state NMR spectral parameters for disordered, heterogeneous, and even amorphous solids (Charpentier et al. 2013).

Here we have used ^{27}Al MAS NMR and ^{27}Al 3QMAS NMR to examine local environments around Al in CaTs. Interpretations of the order-disorder and distortion-or-symmetry of the Al environments observed in the ^{27}Al 3QMAS NMR data can be readily compared with Density Functional Theory computations (CASTEP simulation of NMR parameters) using input crystal structure parameters derived by Rietveld refinement of powder X-ray diffraction data.

EXPERIMENTAL METHODS

Sample preparation

Synthetic Ca-Tschermak (CaTs) pyroxene (RM010K) was prepared from anhydrous glass of stoichiometric proportion, synthesized at 2 GPa and 1400 °C for 24 hours, as described in Flemming and Luth (2002). Sample composition of CaTs (RM010K) was determined by electron probe microanalysis (EPMA) to be $Ca_{1.019(6)}Al_{1.975(13)}Si_{1.006(9)}O_6$. Backscattered electron images of the run product revealed minor (< 1%) corundum and anorthite, as confirmed by EPMA (Flemming and Luth 2002).

Powder XRD and Rietveld crystal structure refinement

Powder X-ray diffraction data was collected on Bruker AXS D8 Advance diffractometer at Western University (London, Ontario), on a 0.5 mm rotating capillary containing approximately 10 mg of sample, using CuKα radiation (λ=1.5418 Å), a Gobel

mirror parallel optics system, and scintillation counter, in theta-theta geometry (Flemming, 2007).

The crystal structures were refined using Topas 3.0 software (Bruker-AXS). Starting parameters for the crystal structure refinement of CaTs (RM010K) were taken from Okamura et al. (1974) and composition was assumed to be ideal $CaAlAlSiO_6$. Within space group C2/c (Z=4), Ca fully occupies M2 at position 4e, Al fully occupies the M1 at position 4e, whereas Si and Al share the tetrahedral site (occupancy 0.5 each) at position 8f. The three oxygen positions (all position 8f) were assumed to be fully occupied. The refined atomic parameters are listed in Table 1.

Note that the crystal structure refinement was significantly improved by incorporation of size/strain parameters (see Table 1). There was no significant preferred orientation owing to data collection in a rotating capillary. The capillary, however, added a 'glass hump' to the pattern which was modeled by adding a 'peaks phase'.

Quartz was also identified by X-ray diffraction of the powdered sample. Quartz (space group P3221) was added to the refinement, using atomic coordinates from Levien et al. (1980) (at 1 atm). Scale, unit cell parameters and profile parameters were refined. Atomic positions remained fixed. Modal analysis yielded 1.5(3) % quartz. Quartz is attributed to having become incorporated during hand grinding of the sample for powder XRD with an agate mortar and pestle. The final run product was hand ground for one hour to ensure particle size < 5 μm, as required for Rietveld-quality data collection. Corundum and anorthite were not detected by X-ray diffraction, owing to their volumetrically minor amounts.

Site size and distortion have been calculated according to Robinson et al. (1971) using VOLCAL (Hazen and Finger 1982) to calculate distortion of cation sites from spherical using quadratic elongation (QE) and angle variance (AV). For this calculation, atomic positions were taken from Table 1. Structures have been drawn using ATOMS software (http://www.shapesoftware.com), using atomic positions from Table 1.

^{27}Al MAS NMR spectroscopy at 14.1 T.

^{27}Al MAS NMR spectra were obtained at Western University (London, Ontario), using a Varian Inova 600 NMR spectrometer at 156.2 MHz (14.1 Tesla; ^{1}H at 600 MHz) with a Varian 3.2 mm HXY MAS probe. Sample spinning frequency was 20.5 kHz. ^{27}Al MAS NMR spectra were acquired using a spectral window of 100 kHz, 2048 data points, and adding 64 scans with a relaxation delay of 30 s; the pulse length was 3.5 μs (1/3 of the liquid 90° r.f. pulse).

^{27}Al MAS NMR and 3QMAS NMR spectroscopy at 21.1 T.

Experiments were performed on a 21.1 T Bruker Avance II NMR spectrometer (^{1}H at 900 MHz) at the Canadian National Ultrahigh-Field NMR Facility for Solids in Ottawa, Ontario, (http://nmr900.ca) using a 3.2 mm Bruker H/X MAS probe. ^{27}Al (Larmor frequency, 234.6 MHz) chemical shifts were referenced to the 1M aqueous solution of $AlCl_3$ ($\delta_{iso} = 0.0$ ppm). For all experiments at 21.1 T, the samples were spun at 22 kHz corresponding to a rotor period of 45.5 μs. One-dimensional ^{27}Al MAS NMR experiments were acquired using a single pulse sequence, with a pulse length of 0.3 μs (about π/6 solid pulse), a recycle delay of 5 s, and 512 transients. The 5 s delay has been

found to be sufficient for complete relaxation. At 21.1 T, ^{27}Al MAS experiments were performed using zirconia (ZrO_2) MAS rotors having negligible ^{27}Al MAS background signal when recorded under the same conditions as the samples.

Two-dimensional ^{27}Al 3QMAS experiments were acquired without rotor synchronization using the spectral width in the indirect F1 dimension of 220 kHz to accommodate all observed chemical shifts. This corresponds to a t_1 increment of the one tenth of one rotor period (4.55 μs). The ^{27}Al 3QMAS NMR experiment used the z-filter pulse sequence proposed by Amoureux et al. (1996). The spectral width in the direct F2 dimension was 100 kHz. For each t_1 increment, 48 transients were accumulated. The total number of t_1 increment was 200. The optimized excitation (P1) and conversion (P2) pulse widths were 3 μs and 1 μs, respectively. At 120 kHz of r.f. power, the ^{27}Al selective 90° pulse width (P3) was 10 μs.

The resulting spectra are Fourier transformed in both t_1 and t_2 time domains, to produce F1 and F2 frequency domains. The F2 dimension contains the MAS spectrum, which preserves the second order quadrupolar broadening. The F1 (3Q) dimension contains a linear combination of isotropic chemical shift (δ_{iso}) and second order quadrupole induced shift (δ_{QIS}). The data have been sheared, to produce the two-dimensional (2D) 3QMAS NMR spectrum, imposing a positive diagonal 1:1 correspondence for the isotropic chemical shifts in the two dimensions.

Measurement and fitting of observed NMR parameters:

Measured NMR parameters were obtained using the C3a convention of Millot and Man (2002).

True isotropic chemical shift (δ_{iso}) is given by equation 3:

$$\delta_{iso} = \frac{10}{27} . \delta_{G2} + \frac{17}{27} . \delta_{G1} \quad \text{.....3}$$

where δ_{G2} is the centre of gravity in the F2 dimension and δ_{G1} is the centre of gravity in the F1 dimension. The quadrupole induced shift (QIS) is given by equation 4:

$$QIS = \delta_{G2} - \delta_{iso} \quad \text{.....4}$$

The second order quadrupole effect (SOQE) is given by equations 5 and 6:

$$SOQE = C_Q \cdot (1 + \eta^2/3)^{1/2} \quad \text{.....5}$$

$$SOQE^2 = QIS . \frac{10}{3} . \frac{[(4I(2I - 1) \nu_o)]^2}{4I (I + 1) - 3} \times 10^{-6} \quad \text{.....6}$$

where η is the asymmetry parameter (see equation 2), ν_o = 234.5 MHz is a natural resonance frequency of ^{27}Al at 21.1 T and I = 5/2.

Selected spectra were also fitted using DMFIT software (Massiot et al. 2002) by varying the quadrupolar coupling constant, C_Q and asymmetry parameter, η. The two methods produced results which agreed well.

Computational Methods to predict NMR parameters by Density Functional Theory (DFT): The CASTEP NMR program (Clark et al. 2005, Profeta et al. 2003) in the Materials Studio 4.4 environment (Accelyrs) was used to calculate ^{27}Al chemical shielding (CS) and electric field gradient (EFG) tensor parameters via ab initio plane-wave density functional theory (DFT). Calculations were performed on a HP xw4400 workstation with a single Intel Dual-Core 2.67 GHz processor and 8 GB DDR RAM. Using the "on-the-fly" method and ultrasoft pseudopotentials provided in CASTEP, ^{27}Al EFG parameters were calculated with a plane wave basis set cutoff energy of 500 eV in a medium accuracy basis set. The Monkhorst-Pack *k*-space grid size of 2×2×4 was used for

all structures. Perdew, Burke, and Ernzerhof (PBE) functionals were employed in the generalized gradient approximation (GGA) for the exchange correlation energy (Perdew et al. 1996, 1998). The magnetic shielding tensors for ^{27}Al were calculated in a medium accuracy basis set using the projector augmented-wave method (GIPAW) (Pickard and Mauri 2001, Yates et al. 2007). No correction was made for the effect of the low energy Ca orbitals (as recommended by Profeta et al. 2004). This may explain a systematic 3-6 ppm difference between the observed and simulated chemical shifts.

Calculations were performed using a geometrically optimized crystallographic structure for CaTs based on the crystal structure reported in this work (Table 1). However, in order to place Al and Si into specific cation sites, a 40-atom segment of the structure was used, having triclinic space group P1. This structural segment contains eight tetrahedral sites (4 Al and 4 Si) as well as four M1 sites (Al), four M2 sites (Ca) and 24 oxygens. This segment maintains charge balanced chemical composition $CaAl(AlSi)O_6$ (Z=4). The eight tetrahedral sites have been selected from four different tetrahedral chains in the structure (A, B, C and D). Every octahedral Al site is connected to six of the eight tetrahedral sites through oxygen, where there are two adjacent sites on the A chain, two adjacent sites on the B chain and one site each from the C chain and the D chain, all bonded to the same octahedral Al. These sites can be occupied by either Al or Si in various arrangements. Placing various Al and Si at the six tetrahedral sites results in three populations of tetrahedral cations around the octahedron, 2Al+4Si, 3Al+3Si and 4Al+2Si (also see Discussion). As adjacent cations on the A and B chains have two different tetrahedral cations in the ordered structure (Al and Si), the four different combinations in total had to be calculated individually. An attempt at having solely Al or Si in the A or the B chain was also made to investigate the influence of disorder on the A

and the B chains. In all cases, the resulting structures were charge balanced by keeping the eight tetrahedral sites filled with four Al and four Si sites.

In the ordered structure, each tetrahedral Al is bonded to three octahedral Al and two tetrahedral Si, leading to an alternating Si-O-Al-O-Si… arrangement on the tetrahedral chain. This is denoted as $(Al)[Al]_3(Si)_2$ (where [ ] and ( ) denote octahedral and tetrahedral cations, respectively). Replacing NNN tetrahedral Si with tetrahedral Al will break the ordered alternating structure, producing disorder on the tetrahedral chain. If both of the NNN Si sites are replaced by tetrahedral Al, this would lead to Al-O-Al-O-Al… clusters on the tetrahedral chain. This extreme end-member of 'disorder' in the structure is defined as $(Al)[Al]_3(Al)_2$.

Replacing only one of the two Si sites with Al (e.g. Al-O-Al-O-Si…) will also break the ordered alternating arrangement, leading to a disordered structure. Replacement of a single Si with Al is energetically more likely than replacement of both NNN Si with Al, as this would produce fewer unfavorable Al-O-Al linkages, which are forbidden by Lowenstein's rule (see Stebbins (1987) for example). This, however, will produce a great number of structures, for Al tetrahedral sites in A, B, C and D chains, which requires a large amount of CASTEP computational resources. Therefore, the CASTEP computation presented here is focused on the completely ordered and completely disordered end-member structures of CaTs. CIF files for the 18 structures used for CASTEP calculations are available as supplementary material.

RESULTS

Crystal structure and site distortion in CaTs

Rietveld crystal structure refinement of the X-ray diffraction data for synthetic CaTs yields space group C2/c, which is consistent with high-temperature CaTs (Okamura et al. 1974). Refined parameters are reported in Table 1 and bond lengths are reported in Table 2. These are in excellent agreement with bond lengths previously reported by Okamura et al. (1974). The crystal structure is shown in Figure 1, with sites labeled. Calculated values for site volume and distortion (QE and AV) are given in Table 3. These are compared with those calculated from Okamura et al. (1974) in Table 3. In CaTs, the tetrahedral site is more distorted than the M1 site. The M2 site is not a regular polyhedron, so M2 distortion parameters could not be calculated by VOLCAL.

^{27}Al MAS NMR spectra at 14.1 and 21.1 T

^{27}Al MAS NMR spectra of CaTs collected at 14.1 and 21.1 T appear in Figure 2a and 2b, respectively. At both field strengths, the ^{27}Al MAS NMR spectrum of CaTs shows two regions of resonance, representing Al at the octahedral and tetrahedral sites. The shoulder at ~16 ppm is attributed to corundum contamination (e.g. Stebbins 1995). This is indicated with an asterisk in Fig. 2.

At both field strengths, the octahedral region (near 0 ppm) displays two well-resolved peaks as well as shoulder features, indicating at least two chemically unique octahedral sites. The well-resolved sites have chemical shift maxima at ~1 and ~6 ppm at 21.1 T. These are displaced by ~ 1 ppm to low frequency (~0 and ~5 ppm) at lower field strength (14.1 T) due to quadrupolar interactions. The two well-resolved octahedral sites observed for the highly aluminous clinopyroxene in this study (CaTs) are not seen in

aluminous orthopyroxenes: Dilute Al in orthoenstatite displays only a single asymmetric site at 18.8 T (Kohn et al. 2005; Palke et al. 2012).

At high field strength (21.1 T) the tetrahedral site (~65 ppm) is broad and asymmetric, suggesting a range of chemical shifts and a relatively large second order quadrupolar interaction. At lower field strength (14.1 T), the tetrahedral peak is resolved into two very broad overlapping peaks (~60 and ~42 ppm). The more pronounced shift in peak position of the lower frequency peak suggests that it is experiencing a larger quadrupole effect. The tetrahedral sites in the spectrum at 14.1 T appear similar to those reported for aluminous orthoenstatite at 18.8 T (Kohn et al. 2005; Palke et al. 2012).

With an increase in field strength, the octahedral and tetrahedral peaks become narrower and their chemical shifts have moved ~1-5 ppm to high frequency (more positive ppm), but the effect is more pronounced for the tetrahedral sites than the octahedral site, indicating that there is a greater quadrupole effect at the tetrahedral sites. The increased broadening and closer proximity of the tetrahedral and octahedral peaks at lower magnetic field strength results in their considerable overlap, illustrating the necessity to acquire ^{27}Al MAS NMR data for aluminous clinopyroxenes at the highest possible magnetic field strength. The severe overlap of the resonances at the tetrahedral site is alleviated by performing ^{27}Al 3QMAS NMR experiments.

^{27}Al 3QMAS NMR spectrum at 21.1 T.

The two-dimensional (2D) ^{27}Al 3QMAS NMR spectrum for CaTs acquired at 21.1 T is shown in Figure 3. Note that the MAS NMR projection (F2) appears across the

top of the figure, above the 2D spectrum, whereas the 3Q indirect dimension (F1) projection is shown on the vertical axis of the 2D spectrum.

F2 spectral slices were taken at five locations along F1, indicated by *a*-*e* in Fig. 3a. The centre of gravity chemical shift (δ_{F1}), isotropic chemical shift (δ_{iso}), quadrupole coupling constant (C_Q), and the asymmetry parameter (η_Q) for each slice are given in Table 4. These values are derived using DMFIT software by Massiot et al. (2002). Also included in Table 4 are measured values for Quadrupole Induced Shift (QIS) and Second Order Quadrupole Effect (SOQE) (as per Millot and Man 2002). SOQE values agreed well with those determined by peak fitting using DMFIT.

Observed NMR parameters at the octahedral site:

Three octahedral environments are well resolved in the 2D ^{27}Al 3QMAS NMR spectrum of CaTs at 21.1 T (Fig. 3a, slices *a*, *b*, and *c*) having true isotropic (fitted) chemical shifts of δ_{iso} = 2.7, 8.6 and 13.5 ppm, and relatively low C_Q (5.0, 4.6 and 5.6, respectively; Table 4). There is also considerable intensity extending to low frequency of the isotropic chemical shift diagonal along F2, which is attributed to additional broadened octahedral sites with large C_Q (~9.1). These additional sites are featured in slices *b* and *c* as peaks *b'* and *c'*, having δ_{iso} = 9.5 and 6.2 ppm, respectively (see Table 4). An additional low-intensity peak appearing at δ_{iso} ~ 22 ppm is attributed to extra-phase corundum. This peak is indicated with an asterisk in Figure 3.

Observed NMR parameters at the tetrahedral site:

At 21.1 T, the 2D ^{27}Al 3QMAS NMR spectrum of the tetrahedral region of CaTs exhibits two distinct tetrahedral resonances. These resonances are well resolved in two dimensions (Fig. 3, slices *d* and *e*). Slice *d* shows a single peak centred at ~ 65 ppm in F1. This peak is broad in F1 and F2, suggesting a dispersion of chemical shifts due to a variety of tetrahedral environments under the chemical shift envelope, as indicative of cation disorder. All intensity lies approximately on the isotropic chemical shift diagonal of the 3QMAS NMR spectrum, showing that this tetrahedral site is little affected by the quadrupolar interactions (C_Q=5.4), and is most likely a symmetric AlO_4 polyhedron.

A second tetrahedral peak (Fig. 3, slice *e*) appears very broad in F2, but is considerably narrower in F1; it is centred at ~ 80 ppm in F1. Its narrow width in F1 suggests that this site contains a high degree of cation order. The considerable intensity along F2 can be fitted with one very broad peak (labelled peak *e* in Fig. 4) having a high quadrupolar coupling constant (11.8 MHz), indicative of a highly-distorted site. Site distortion is consistent with the reported value for Quadratic Elongation (QE = 1.0085), which is relatively high for a tetrahedral site. Notably, this highly-distorted region was not detected by ^{27}Al 3QMAS NMR at lower field strength (e.g. at 11.7 T: Flemming and Wu, 2002), likely due to inefficient excitation and conversion of broad (high C_Q) MQ resonances. For this reason, at lower field, extremely broad (high C_Q) resonances may be observed in MAS experiments but will fail to be observed during MQMAS experiments.

Results of DFT Calculations:

Table 5 presents ^{27}Al 3QMAS NMR parameters calculated using Density Functional Theory (DFT) for two end-member structures of CaTs ($Ca[Al](AlSi)O_6$)

labeled 'ordered' and 'disordered'. Consistent with the crystal structure, the model uses six next nearest neighbor (NNN) tetrahedral sites around an octahedral Al site, in which the tetrahedral sites can have three cation populations: 2Al+4Si, 3Al+3Si, and 4Al+2Si. Their structures can be either ordered or disordered. The completely ordered tetrahedral environment around Al in both the tetrahedral and M1 sites is created from a tetrahedral chain containing alternating Si-O-Al-O-Si… linkages; this ordered configuration is labelled $(Al)[Al]_3(Si)_2$ (where [ ] and ( ) denote octahedral and tetrahedral cations, respectively). Replacing Si with Al at both sites on the tetrahedral chain creates an end-member 'disordered' tetrahedral environment around Al in both the tetrahedral and M1 sites, where the tetrahedral chain contains Al-O-Al-O-Al… linkages; this disordered configuration is labelled $(Al)[Al]_3(Al)_2$.

Simulated ^{27}Al 3QMAS NMR parameters - centre of gravity chemical shift in F1 (δ_{CG} of F1), isotropic chemical shift (δ_{iso}), quadrupole coupling constant (C_Q), and the asymmetry parameter (η_Q) - are given in Table 5 for both the octahedral and tetrahedral sites, with predictions for both the disordered and the ordered structural models. These DFT simulated parameters for ordered and disordered CaTs are used below to guide the discussion of the fitted parameters for the observed NMR spectra.

DISCUSSION

Local environments around tetrahedral and octahedral Al:

Consider the local environment around the tetrahedral cation, as shown in Fig. 1. This conventional view of the pyroxene crystal structure clearly shows the nine next

nearest neighbor (NNN) cations around the tetrahedral site. Each tetrahedral Al in the structure is bonded to two corner sharing NNN tetrahedra (Si or Al) in the single chain through O3, three NNN octahedral Al cations at M1 (two through O1 and one through O2) as well as four Ca cations at the eight-coordinated M2 site. In Fig. 1, the bonds from one tetrahedral cation to the M1 and M2 cations have been indicated in red to illustrate the coordination environment.

Fig. 5a aids visualization of the local cation environments around octahedral Al in the M1 site. This alternative view of the CaTs crystal structure is oriented to feature the octahedral M1 site and its eight closest NNN cations - six NNN tetrahedral cations (Al or Si) from four tetrahedral chains (TA, TB, TC and TD) sharing corners with the M1 octahedron, and two octahedral cations on the M1 chain, sharing edges with the M1 octahedron (bonds not shown in Fig. 5). In CaTs, the M1 sites are solely occupied by Al. Therefore, the octahedral sites are fully ordered, and adjacent octahedral sites can be ignored during subsequent discussion about cation ordering. Note that the edge-sharing M2 chain is entirely occupied by Ca, and as cation substitution is not occurring at the M2 site, it is omitted from the discussion below. In Fig. 5, the M2 sites have been omitted for simplicity.

Each M1 cation is connected to six corner-shared tetrahedral sites from four different tetrahedral chains: Two tetrahedral sites from the A chain (TA) through O1, two from the B chain (TB) through O1, and one from each of the C and D chains (TC and TD, respectively) through O2. The six tetrahedral sites in CaTs can be occupied by Si or Al in equal proportion, according to structural formula $Ca[Al](AlSi)O_6$, where [ ] and ( ) indicate octahedral and tetrahedral sites, respectively. The tetrahedral cation distribution

around Al in M1 will be annotated as TATA-TBTB-TC-TD. In the case of complete ordering on the tetrahedral chain (i.e. alternating Si-O-Al-O-Si…) there are three possible combinations of tetrahedral cations around M1. These are SiAl-SiAl-Si-Si, SiAl-SiAl-Si-Al (≡ SiAl-SiAl-Al-Si) and SiAl-SiAl-Al-Al. This leads to three populations among the six tetrahedral sites around M1: 2Al+4Si, 3Al+3Si and 4Al+2Si, respectively. These three ordered environments are pictured in Fig. 5. b-d. Note that exchanging the order in TATA and TBTB from SiAl to AlSi would generate an additional three sites having the same Si/Al ratios as the previously described sites.

Interpretation of octahedral Al in the ^{27}Al 3Q MAS NMR spectrum:

The ^{27}Al 3QMAS NMR spectrum of CaTs at 21.1 T (Fig. 3) contains three well-resolved octahedral peaks (a-c) which indicate at least three distinct local environments around Al, all having relatively low C_Q. Because all octahedral sites contain Al, the octahedral chain is fully ordered and cannot contribute to multiple sites. This means that Al in the octahedral site is sensitive to substitution of Al for Si on the six surrounding tetrahedral sites, as described below.

Octahedral Al environments in a completely ordered structure:

Complete ordering on the tetrahedral chain is a reasonable first approximation, as we know from ^{29}Si MAS NMR spectra of CaTs (Flemming and Luth 2002) that 70% of Si in the chain is ordered locally into environments of alternating Al-O-Si-O-Al. Assuming that Al and Si are equally likely to be present on TC and TD sites, the three unique ordered environments may be portrayed as 2Al+4Si, 3Al+3Si, and 4Al+2Si, with

relative proportions of 1:2:1 (being SiAl-SiAl-Si-Si, SiAl-SiAl-Si-Al (≡ SiAl-SiAl-Al-Si) and SiAl-SiAl-Al-Al). By this statistical argument, the observed peak with the highest intensity, at δ_{iso} = 8.6 ppm (Fig. 3 and 4b, slice *b*), should represent the 3Al+3Si arrangement. The peaks to either side of this, at δ_{iso} = 2.7 and 13.5 ppm (Fig. 3 and 4, slices *a* and *c*, respectively) are assigned to 2Al+4Si, and 4Al+2Si, respectively, assuming that substitution of Al for Si at a neighboring cation position around M1 produces deshielding of Al, similar to that observed for Si in ^{29}Si NMR spectra (Flemming and Luth 2002). Note that peak *b* is not twice the intensity of the other two peaks for two possible reasons: the tetrahedral chain is not fully ordered, and MQ MAS NMR spectra are not strictly quantitative.

DFT results for octahedral Al in a completely ordered structure:

When modeling the octahedral site using a completely ordered structure, $(Al)[Al]_3(Si)_2$, octahedral Al sites surrounded by the three NNN tetrahedral cation environments, 2Al+4Si, 3Al+3Si and 4Al+2Si, show both high C_Q (7.6 - 9.1 MHz) and low C_Q (1.7 - 5.3 MHz) environments, depending on the ordering of Al sites in the A and B chains. When the C_Q is low, the Al peak positions at F1 follow the trend: 2Al+4Si < 3Al+3Si < 4Al+2Si. This is consistent with the assumption that substitution of Al for Si at the neighboring tetrahedral cation position produces deshielding of Al, which shifts the peak to higher chemical shift. Nevertheless, when C_Q is high, the quadrupolar induced shift changes the peak position at F1. This results in mixed peak positions for the three coordination environments, ranging from 6.3 to 9.5 ppm depending on the C_Q values (see Table 5), which makes them impossible to resolve.

The local arrangement of 3Al+3Si is consistent with the tetrahedral cation distribution that would occur around M1 in the fully-ordered structure with space groups $P2_1/n$ and C-1 (Okamura et al. 1974), whereas the fully-ordered structure with space groups P2/n and C2 (Okamura et al. 1974) would contain equal populations of 2Al+4Si and 4Al+2Si in the six tetrahedral sites around M1. Cohen and Burnham (1985) predicted $P2_1/n$ to be the most energetically favorable ordered configuration based on energy calculations, with C2 being the second most favorable ordered configuration. This suggests that the disordered high-temperature structure possesses locally ordered domains consistent with both the $P2_1/n$ and C2 long-range ordered structures.

Octahedral Al environments in a completely disordered structure:

Note slice *b* and *c* contain additional peaks with high C_Q (peaks *b'* and *c'* in Fig. 4 b-c). These peaks are likely comprised of additional NNN populations arising from disorder and site distortion, possibly associated with Al-O-Al linkages. Flemming and Luth (2002) also found 13% Al-O-Al linkages (= Si-O-Si) in CaTs by ^{29}Si MAS NMR. If disorder is incorporated onto the tetrahedral chain, the number of possible environments around M1 increases from three to 15, because TATA-TBTB can also include SiSi-SiSi, SiSi-SiAl, SiSi-AlAl, AlAl-AlSi, and AlAl-AlAl (assuming SiAl and AlSi to be equivalent). Disorder in the tetrahedral chain, such as Al-O-Al and Si-O-Si linkages, would change the population ratios of the three assigned peaks. This might contribute to the additional intensity to low frequency in slices *b* and *c* (see Fig. 3); Site distortion potentially occurring around the Al-O-Al sites would contribute to the higher

C_Q of these sites. However, a quantitative treatment of the peak intensities is not possible at this point.

DFT results for octahedral Al in an end-member disordered structure:

When modeling the end-member disordered structure, $(Al)[Al]_3(Al)_2$, the octahedral Al sites having tetrahedral NNN population 2Al+4Si and 4Al+2Si show only low C_Q (2.9 - 4.0 MHz), whereas those from 3Al+3Si show both low C_Q (3.0 MHz) and high C_Q (7.7 MHz; see Table 5), related to the ordering of Al sites in the A and B chains. Similar to the case of the completely ordered structure discussed above, when the C_Q is low, the Al peak positions at F1 follow the same trend of 2Al+4Si < 3Al+3Si < 4Al+2Si. When C_Q is high, the peak position at F1 still falls in the region of 6.3 - 9.5 ppm.

Interpretation of ^{27}Al 3QMAS NMR of tetrahedral Al environments – two extremes:

The ^{27}Al 3QMAS NMR spectrum at 21.1 T shows two tetrahedral regions of interest (Fig 3 and 4, slices *d* and *e*). The peak at δ_{iso} = 66.5 ppm (Fig 3, slice *d*) demonstrates spreading of the signal along the isotropic chemical shift line. This broadening is likely due to a distribution of chemical shifts attributed to cation disorder on the tetrahedral site, consistent with Flemming and Luth's (2002) report of 30% disorder in CaTs. The geometry of the first tetrahedral site (Figs. 3 and 4, slice *d*) appears to be fairly symmetric, given that its signal intensity does not extend in the F2 direction as would be the case for a high quadrupolar interaction. A second tetrahedral region centred at δ_{iso} = 79.7 ppm (Figs. 3 and 4, slice *e*) appears narrow in F1 suggesting a high degree of cation order, but it exhibits extensive spreading in the F2 dimension,

indicative of a high quadrupole coupling constant (C_Q = 11.8 MHz), which suggests high site distortion.

Following the peak assignment strategy for the tetrahedral sites in gehlenite by Florian et al. (2012), an increase in the number of tetrahedral Al NNN causes the chemical shift to move to higher frequency (more positive values); thus, the relative chemical shifts of peaks *d* and *e* (66.5 vs. 79.7 ppm, respectively) suggest that there is more Al surrounding peak *e* than peak *d*. A higher Al content also appears correlated with higher site distortion (higher C_Q).

This highly-distorted site (peak *e*) was not detected by ^{27}Al 3QMAS NMR at lower field strength (e.g. at 11.7 T: Flemming and Wu, 2002), suggesting that CaTs contains highly distorted tetrahedral sites that cannot be observed by ^{27}Al 3QMAS NMR at lower magnetic field strengths. The measured C_Q of 11.8 is in the order of that for the octahedral site in andalusite (C_Q = 15.3) which has been classically challenging to observe (Rocha 1998; Alemany et al. 1999; Kanellopoulos et a. 2007).

DFT results for tetrahedral Al in a completely ordered structure:

Ordered tetrahedral Al sites all show high C_Q (9.5 - 10.2 MHz). This may be attributed to Al-O-Al linkages in the structure $(Al)[Al]_3(Si)_2$. The DFT modeled high C_Q of the fully ordered environment is consistent with the observed high quadrupole coupling constant for the ordered tetrahedral site in the ^{27}Al 3Q MAS NMR spectrum (Figs. 3, 4e and Table 4, peak *e*) (C_Q = 8.9 - 10.1 MHz). A large electric quadrupole moment is likely due to high site distortion at this ordered tetrahedral environment, consistent with the observed (fitted) value of C_Q = 11.8 MHz. The observed (fitted)

isotropic chemical shift of peak e, δ_{iso} = 79.7 ppm, is of order ~ 5 ppm higher frequency than the range of DFT simulated values (73.0 - 74.5 ppm), a difference that is most likely an effect of the orbital configuration used in the DFT simulation.

DFT results for tetrahedral Al in an end-member disordered structure:

Contrary to the case of the ordered structure, the tetrahedral Al sites in the disordered structure $(Al)[Al]_3(Al)_2$ all show low C_Q (3.6 - 4.1 MHz). Interestingly, the tetrahedral peak positions at F1 fall into the region of 74.3 - 75.4 ppm which is almost the same as in the case of completely ordered structure $(Al)[Al]_3(Si)_2$. The similarity in Al tetrahedral F1 peak positions results from the contributions by both the increased deshielding from the two neighboring Al sites and the low C_Q which has smaller quadrupolar induced shift as compared with the case of completely ordered structure.

The modeled low C_Q of the fully disordered environment is consistent with the observed low quadrupole coupling (C_Q = 5.4 MHz) measured for the disordered tetrahedral site in the ^{27}Al 3QMAS NMR spectrum (Fig. 3 and Table 4, peak *e*), suggesting low site distortion at this disordered tetrahedral environment. The measured true isotropic chemical shift, of δ_{iso} = 66.5 ppm, is considerably lower than the range of simulated values (74.3 - 75.4 ppm), but the observed peak is very broad in its extent along F1 as well as along the isotropic chemical shift diagonal line, demonstrating that there is considerable chemical shift distribution associated with these disordered sites.

In summary, there appear to be two types of tetrahedral environment in CaTs: a relatively undistorted symmetric site which exhibits a high degree of cation disorder

around Al (Figs. 3 and 4, slice *d*), and a highly distorted region (Figs. 3 and 4, slice *e*) which appears to contain considerable cation ordering around Al. The high degree of quadrupolar broadening in slice *e*, attributed to significant site distortion, appears to render this site impossible to detect by ^{27}Al 3QMAS NMR at lower field strength than 21.1 T.

Summary and predictions from computational results:

It appears that in ^{27}Al NMR spectra, the tetrahedral Al site is the most sensitive indicator of order/disorder in CaTs. Tetrahedral Al sites in fully ordered tetrahedral chains (Si-O-Al-O-Si…) exhibit large C_Q (Fig. 3, peak *e*), whereas tetrahedral Al sites in disordered systems (Al-O-Al-O-Al…) appear to have only small C_Q (Fig. 3, peak *d*). Both environments appear to exist in CaTs (Fig. 3, peaks *d* and *e*). The high C_Q for ordered chains in CaTs is consistent with its high Quadratic Elongation parameter (distortion from spherical) for the tetrahedral site in CaTs, of QE=1.0085 (Table 3). High QE indicates that the tetrahedral site is quite distorted for the pyroxene structure, second only to orthoenstatite, which has QE=1.0099 (Cameron and Papike 1981). Although the structure is long range disordered (C2/c) it shows a high degree of local ordering according to ^{29}Si MAS NMR, where 70% of the chain is ordered into alternating Ai-O-Si-O-Al... tetrahedra (Flemming and Luth 2002).

Octahedral Al bonded to the six tetrahedral cations in three combinations (2Al+4Si, 3Al+3Si, 4Al+2Si), fall into two groups, those having larger C_Q (8-9 MHz) or smaller C_Q (4-5 MHz); both ranges of C_Q occur for various cation combinations in the ordered structure, as well as for the 3Al+3Si cation combination in the disordered

structure. Thus, C_Q of the octahedral site would not be a useful indicator of order-disorder in the structure.

C_Q is predicted to be always small for octahedral sites surrounded by combinations of 2Al+4Si or 4Al+2Si cations in the disordered structure. For octahedral sites with small C_Q (narrow resonances), δ_{iso} follows the predicted trend: δ_{iso} (2Al+4Si) < δ_{iso} (3Al+3Si) < δ_{iso} (4Al+2Si). However octahedral sites with large C_Q do not follow this trend, because large C_Q moves δ_{G1} into more positive chemical shifts, which thus overlap. These sites most likely form the broad resonance spreading to the right of the maxima of the octahedral sites in the ^{27}Al 3QMAS spectrum (Fig. 3) and cannot be resolved.

The sensitivity of ^{27}Al 3QMAS NMR to substitution of Mg for Al on the octahedral sublattice was not measured in this study, as CaTs contains only Al at the octahedral site. Further systematic study by ^{27}Al 3QMAS NMR across the diopside-CaTs solid solution is underway to observe the effects of tetrahedral Si-Al versus octahedral Mg-Al substitution on ^{27}Al NMR peak position and quadrupole coupling, C_Q.

IMPLICATIONS

The ^{27}Al 3QMAS NMR spectrum of CaTs at 21.1 T (Fig 3) has revealed that octahedral Al is sensitive to Si-Al substitution in the six surrounding tetrahedral sites, displaying at least three well-resolved octahedral Al environments with proposed peak assignments of 2 Al + 4 Si, 3 Al + 3 Si and 4 Al + 2 Si. Multiple peaks in ^{27}Al 3QMAS NMR of CaTs indicate short-range ordered environments within the disordered high-temperature C2/c structure, reminiscent of the four long-range ordered tetrahedral cation

arrangements envisaged for CaTs by Okamura (1974): C2, P2/n, C-1and $P2_1/n$. This implies that a high degree of short-range ordering is occurring locally on the tetrahedral chain, despite the phase transition to ordered structures (e.g. $P2_1/n$ as predicted by Cohen 1986, Bosenik et al. 2001) being predicted to not occur until temperatures well below the stability field of aluminous clinopyroxene (727 °C: Bosenick et al. 2001, Warren et al. 2001).

^{27}Al 3QMAS NMR could also be used to discern between ordered structures. An ordered $P2_1/n$ structure (as predicted by Cohen 1986; Bosenick 2001) with M1 surrounded by 3Al + 3Si should consist of a single octahedral peak and a tetrahedral peak with high C_Q indicative of an ordered environment. C2 on the other hand (as predicted by Cohen and Burnham 1985; Cohen 1986) would contain two octahedral peaks and two tetrahedral peaks (with variable C_Q), representing the two environments having 4Al + 2Si and 2Al + 4Si. The existence of significant short-range ordering in the tetrahedral sites in CaTs, first observed by ^{29}Si MAS NMR (Flemming and Luth 2002), will significantly decrease the configurational entropy contribution to the free energy of clinopyroxenes containing significant CaTs component. This will need to be taken into account for CaTs-containing thermobarometers used in mantle petrology. This is also of importance in planetary science, as CaTs (also called kushiroite (Kimura et al. 2009)) is an important component of Calcium Aluminum-rich Inclusions (CAIs) in chondritic meteorites, and its cation order-disorder may record information about temperatures in the solar nebula.

^{27}Al 3QMAS NMR at 21.1 T has exposed a previously NMR-invisible tetrahedral site with very high C_Q, attributed to extremely high site distortion. The implication of this discovery is that many silicate mineral solid solutions potentially have very distorted

sites created by cation substitution. These sites may not have been observed by NMR at lower magnetic field strengths and ^{27}Al MAS NMR spectra of potentially distorted aluminosilicate minerals will need to be re-acquired at the highest possible magnetic field strength.

ACKNOWLEDGEMENTS

This work was made possible by Natural Sciences and Engineering (NSERC) Discovery grant funding to RLF and Canadian Foundation for Innovation (CFI) funding to the National Ultrahigh-field NMR Facility for Solids. We wish to thank R.W. Luth (University of Alberta) for support for mineral synthesis, and M. Willans for acquiring ^{27}Al MAS NMR data at 600 MHz at Western University. We also wish to thank T. Nakashima (University of Alberta) for preliminary data at 300 MHz, C. Kirby (Western University) for preliminary data at 400 MHz, G. Wu (Queen's University) for preliminary data at 500 MHz, W. Power (University of Waterloo) for preliminary data at 600 MHz, and S. Pawsey (University of Ottawa) for assistance at 900 MHz. We are grateful to P. J. A. McCausland for reading the manuscript and for useful discussions. We wish to thank P. Boyle, R. Peterson and R. Angel for help with CIF files. We also wish to thank Editor K. D. Putirka, Associate Editor B. L. Phillips, Technical Editor R. J. Angel and three anonymous reviewers for their useful comments, which have greatly improved the manuscript.

REFERENCES CITED

Alemany, L.B., Callender, R.L., and Barron, A.R., (2000) Single-pulse MAS, selective Hahn echo MAS, and 3QMAS NMR studies of the mineral zoisite at 400, 500, 600, and 800 MHz. Exploring the limits of Al NMR detectability. *Journal of Physical Chemistry B*, 104, 11612-11616.

Alemany, L.B., Steuernagel, S., Amoureux, J.-P., Callender, R.L., and Barron, A.R. (1999) Very fast MAS and MQMAS NMR studies of the spectroscopically challenging minerals kyanite and andalusite on 400, 500, and 800 MHz spectrometers. *Solid State Nuclear Magnetic Resonance*, 14, 1-18.

Amoureux, J.-P., Fernandez, C., and Steuernagel, S. (1996) Z-filtering in MQMAS NMR. *Journal of Magnetic Resonance, Series A*, 123, 116-118.

Ashbrook, S.E., McManus, J., MacKenzie, K.J.D., and Wimperis, S. (2000) Multiple-quantum and cross-polarized Al-27 MAS NMR of mechanically treated mixtures of kaolinite and gibbsite. Journal of Physical Chemistry B, 104, 6408-6416.

Ashchepkov, I.V. (2002) An empirical clinopyroxene thermobarometer for mantle rocks based on the jadeite-diopside exchange. *Doklady Earth Sciences*, 382, 78-82.

Baltisberger, J.H., Xu, Z., Stebbins, J.F., Wang, S.H., and Pines, A. (1996) Triple-quantum two-dimensional ^{27}Al Magic-angle spinning nuclear magnetic resonance study of aluminosilicate and aluminate crystals and glasses. *Journal of the American Chemical Society*, 118, 7209-7214.

Biswal, M., Body, M., Legein, C., Corbel, G., Sadoc, A., and Boucher, F. (2012) Structural Investigation of α- and β-Sodium Hexafluoroarsenate, NaAsF6, by Variable Temperature X-ray Powder Diffraction and Multinuclear Solid-State

NMR, and DFT Calculations. *Journal of Physical Chemistry C*, 116, 11682-11693.

Bonhomme, C., Gervais, C., Babonneau, F., Coelho, C., Pourpoint, F., Azaïs, T., Ashbrook, S.E. Griffin, J. M., Yates, J.R., Mauri, F., and Pickard, C.J. (2012) First-Principles Calculation of NMR Parameters Using the Gauge Including Projector Augmented Wave Method: A Chemist's Point of View. *Chemical Reviews*, 112, 5733−5779.

Bosenick, A., Dove, M.T., Myers, E.R., Palin, E.J., Sainz-Diaz, C.I., Guiton, B.S., Warren, M.C., Craig, M.S., and Redfern, S.A.T. (2001) Computational methods for the study of energies of cation distributions: applications to cation-ordering phase transitions and solid solutions. *Mineralogical Magazine*, 65, 193-219.

Brearley, A.J., and Jones, R.H. (1998) Chondritic Meteorites. In J.J. Papike, Ed., Planetary Materials. Reviews in Mineralogy, 36, 3-1 – 3-370.

Cameron, M., and Papike, J.J. (1981) Structural and chemical variation in pyroxenes. *American Mineralogist*, 66, 1-50.

Charpentier, T., Menziani, M.C., and Pedone, A. (2013) Computational simulations of solid state NMR spectra: a new era in structure determination of oxide glasses. *RSC Advances*, 3, 10550 - 10578 and references therein.

Choi, M., Matsunaga, K., Oba, F., and Tanaka, I. (2009) ^{27}Al NMR Chemical Shifts in Oxide Crystals: A First-Principles Study. *Journal of Physical Chemistry C*, 113, 3869-3873.

Clark, S.J., Segall, M.D., Pickard, C.J., Hasnip, P.J., Probert, M.J., Refson, K., Payne, M.C. (2005) First principles methods using CASTEP. *Zeitschrift fuer Kristallographie*, 220, 567-570.

Cohen, R.E. (1986) Configurational Thermodynamics of Aluminous Pyroxenes: A Generalized Pair Approximation. *Physics and Chemistry of Minerals,* 13, 183-197.

Cohen, R.E., and Burnham, C.W. (1985) Energetics of ordering in aluminous pyroxenes. *American Mineralogist*, 70, 559-567.

Damodaran, K., Rajamohanan, P.R., Chakrabarty, D., Rachelra, U.S., Manohar, V. Fernandez, C., Amoureux, J.-P., and Ganapthy, S. (2002) Triple-quantum magic angle spinning Al-27 NMR of aluminum hydroxides. *Journal of the American Chemical Society*, 124, 3200-3201.

Dal Negro, A., Carbonin, S., Salviulo, G., Piccirillo, E.M., and Cundari, A. (1985) Crystal chemistry and site configuration of the clinopyroxene from leucite bearing rocks and related genetic significance: The Sabatini lavas, Roman region, Italy. *Journal of Petrology*, 26, 1027–1040.

Dal Negro, A., Cundari, A., Piccirillo, E.M., Molin, G.M., and Uliana, D. (1986) Distinctive crystal chemistry and site configuration of the clinopyroxene from alkali basaltic rocks. The Nyambeni clinopyroxene suite, Kenya. *Contributions to Mineralogy and Petrology*, 92, 35–43.

Deer, W.A., Howie, R.A., and Zussman, J. (1978) *Rock-Forming Minerals Volume 2A: Single Chain Silicates*. 2nd ed. Longman Group Limited, London. UK. 668 pp.

Dowty, E., and Clark, J.R. (1973) Crystal structure refinement and optical properties of a Ti^{3+} fassaite from the Allende meteorite. *American Mineralogist*, 58, 230-242.

Durazzo, A. (1999) Using Mineralogy in the petrogenesis of ultramafic tocks: Examples from Italy. *International Geology Review*, 41, 175-190.

Etzel, K. Benisek, A., Dachs, E., and Cemic, L. (2007) Thermodynamic mixing in synthetic CaTs-diopside solid solution I. Volume and heat capacity of mixing. *Physics and Chemistry of Minerals*, 34, 733-746.

Ferrara, C., Tealdi, C., Pedone, A., Menziani, M.C., Rossini, A.J., Pintacuda,G., and Mustarelli, P. (2013) Local versus Average Structure in $LaSrAl_3O_7$: A NMR and DFT Investigation. *Journal of Physical Chemistry C*, 117, 23451-23458.

Flemming, R.L., and Luth, R.W. (2002) ^{29}Si MAS NMR study of diopside – Ca-Tschermak clinopyroxenes: Detecting both tetrahedral and octahedral Al. *American Mineralogist*, 87, 25-36.

Flemming, R.L., and Wu, G. (2002) Direct evidence of ordered octahedral environments in diopside-CaTs clinopyroxenes, from ^{27}Al 3QMAS NMR. *International Mineralogical Association 18th General Meeting*, MS8, p. 85 (Sept 1-6, 2002)

Florian, P., Veron, E., Green, T.F.G., Yates, J.R., and Massiot, D. (2012) Elucidation of the Al/Si ordering in gehlenite $Ca_2Al_2SiO_7$ by combined ^{29}Si and ^{27}Al NMR spectroscopy/ quantum chemical calculations. *Chemistry of Materials*, 24, 4068–4079.

Frydman, L., and Harwood, J.S. (1995) Isotropic spectra of half-integer quadrupolar spins from bidimensional magic-angle spinning NMR, *Journal of the American Chemical Society*, 117, 5367-5368.

Gaeta, M., Di Rocco, T., and Freda, C. (2009) Carbonate assimilation in open magmatic systems: the role of melt-bearing skarns and cumulate-forming processes. *Journal of Petrology*, 50, 361-385.

Gambuzzi, E., Pedone, A., Menziani, M.C., Angeli, F., Caurant, D., and Charpentier, T. (2014) Probing silicon and aluminium chemical environments in silicate and aluminosilicate glasses by solid state NMR spectroscopy and accurate first-principles calculations. *Geochimica et Cosmochimica Acta*, 125, 170-185.

Gore, K.U., Abraham, A., Hegde, S.G., Kumar, R., Amoureux, J.-P., and Ganapthy, S. (2002) Si-29 and Al-27 MAS/3Q-MAS NMR studies of high silica USY zeolites. *Journal of Physical Chemistry B*, 106, 6115-6120.

Grove, T.L., and Burnham, C.W. (1974) Al-Si disorder in Calcium Tschermak's pyroxene, $CaAl_2SiO_6$. *EOS, Transactions of the American Geophysical Union*, 56, 1202 (abstract).

Hawthorne, F.C., Welsh, M.D., Della Ventura, G., Liu, S., Robert, J.-L., and Jenkins, D.M. (2000) Short-range order in synthetic aluminous tremolites: An infrared and triple-quantum MAS NMR study. *American Mineralogist*, 85, 1716-1724.

Hays, J. F. (1966) Lime-alumina-silica. *Carnegie Inst. Washington Year Book*, 65: 234-239.

Hazen, R.M., and Finger, L.W. (1982) *Comparative Crystal Chemistry: Temperature, pressure, composition, and the variation of crystal structure.* Wiley, New York, 231 p.

Hazen, R.M., and Finger, L.W. (1977) Crystal structure and compositional variation of Angra dos Reis fassaite. *Earth and Planetary Science Letters*, 35, 357-362.

Kanellopoulos, J., Freudea, D., and Kentgens, A. (2007) A practical comparison of MQMAS techniques. *Solid State Nuclear Magnetic Resonance*, 32, 99–108.

Kimura, M., Mikouchi, T., Suzuki, A., Miyahara, M., Ohtani, E., and El Goresy, A. (2009) Kushiroite, CaAlAlSiO6: A new mineral of the pyroxene group from the ALH 85085 CH chondrite, and its genetic significance in refractory inclusions. *American Mineralogist*, 94, 1479–1482.

Kirkpatrick, J. (1988) MAS NMR spectroscopy of minerals and glasses. in Hawthorne Ed. Spectroscopy in Mineralogy and Geology. *Reviews in Mineralogy*, 18, 341.

Kogiso, T., Hirschmann, M.M., and Pertermann, M. (2004) High-pressure partial melting of mafic lithologies in the mantle. *Journal of Petrology*, 45, 2407-2422.

Kohn, S.C., Roome, B.M., Smith, M.E., and Howes, A.P. (2005) Testing a potential mantle geohygrometer; the effect of dissolved water on the intracrystalline partitioning of Al in orthopyroxene. *Earth and Planetary Science Letters*, 238, 342–350.

Levien, L., Prewitt, C. T., and Wiedner, D. J. (1980) Structure and elastic properties of quartz at pressure. *American Mineralogist*, 65, 920-930.

Ma, C., Simon, S.B., Rossman, G.R., and Grossman, L. (2009) Calcium Tschermak's pyroxene, $CaAlAlSiO_6$, from the Allende and Murray meteorites: EBSD and micro-Raman characterizations. *American Mineralogist*, 94, 1483–1486.

Massiot, D., Fayon, F., Capron, M., King, I., Le Calve, S., Alonso, B., Durand, J.-O., Bujoli, B., Gan, Z., and Hoatson, G. (2002) Modelling one- and two-dimensional solid-state NMR spectra. *Magnetic Resonance in Chemistry*, 40, 70-76.

Millot, Y., and Man, P.P. (2002) Procedures for Labeling the High-Resolution Axis of Two-Dimensional MQ-MAS NMR Spectra of Half-Integer Quadrupole Spins. *Solid State Nuclear Magnetic Resonance*, 21, 21-43.

Mittlefehldt, D.W., Killgore, M., and Lee, M.T. (2002) Petrology and geochemistry of D'Orbigny, geochemistry of Sahara 99555, and the origin of angrites. *Meteoritics and Planetary Science*, 37, 345-369.

Millard, R.L., and Luth, R.W. (1998) Tetrahedral Si/Al distribution in Di-CaTs clinopyroxenes using ^{29}Si MAS NMR. *EOS Transactions of the American Geophysical Union*, 79, S162.

Mollo, S., Gaeta, M., Freda, C., Di Rocco, T., Misiti, V., and Scarlato, P. (2010) Carbonate assimilation in magmas: A reappraisal based on experimental petrology. *Lithos*, 114, 503-514.

Nimis, P. (1995) A clinopyroxene geobarometer for basaltic systems based on crystal-structure modeling. *Contributions to Mineralogy and Petrology*, 121, 115-125.

Nimis, P. (1999) Clinopyroxene geobarometry of magmatic rocks. Part 2. Structural geobarometers for basic to acid, tholeiitic and mildly alkaline magmatic systems. *Contributions to Mineralogy and Petrology*, 135, 62-74.

Nimis, P., and Ulmer, P. (1998) Clinopyroxene geobarometry of magmatic rocks. Part 1. An expanded structural geobarometer for anhydrous and hydrous, basic and ultrabasic systems. *Contributions to Mineralogy and Petrology*, 133, 122-135.

Okamura, F.P., Ghose, S., and Ohashi, H. (1974) Structure and crystal chemistry of calcium Tschermak's pyroxene, $CaAlAlSiO_6$. *American Mineralogist*, 59, 549-557.

Palke, A.C., Stebbins, J.F., Frost, D.J., and McCammon, C.A. (2012) Incorporation of Fe and Al in $MgSiO_3$ perovskite: An investigation by ^{27}Al and ^{29}Si NMR spectroscopy. *American Mineralogist*, 97, 1955-1964.

Pascal, M.-L., Katona, I., Fonteilles, M., and Verkaeren, J. (2005) Relics of high temperature clinopyroxene on the join Di–CaTs with up to 72 mol % $Ca(Al,Fe^{3+})AlSiO_6$ in the skarns of Ciclova and Magureaua Vatei, Carpathians, Romania. *Canadian Mineralogist*, 43, 857–881.

Peacor, D.R. (1967) Refinement of the crystal structure of a pyroxene of formula $M_IM_{II}(Si_{1.5}Al_{0.5})O_6$. *American Mineralogist*, 52, 31-41.

Pedone, A., Charpentier, T., and Menziani, M.C. (2010) Multinuclear NMR of $CaSiO_3$ glass: simulation from first-principles. *Physical Chemistry Chemical Physics*, 12, 6054–6066.

Pedone, A., Gambuzzi, E., Malavasi, G., and Menziani, M.C. (2012) First-principles simulations of the 27Al and 17O solid-state NMR spectra of the CaAl2Si3O10 glass. *Theoretical Chemistry Accounts*, 131, 1147-1158.

Perdew, J.P., Burke, K., and Ernzerhof, M. (1996) Generalized Gradient Approximation Made Simple. *Physics Review Letters*, 77, 3865-3868.

Perdew, J.P., Burke, K., and Ernzerhof, M. (1998) *Physics Review Letters*, 80, 891-894. Reply to the Comment by Y. Zhang and W. Yang on “Generalized Gradient Approximation Made Simple".

Pickard, C.J., and Mauri, F. (2001) All-electron magnetic response with pseudopotentials: NMR chemical shifts. *Physical Review B63*, 245101.

Profeta, M., Mauri, F., and Pickard, C. J. (2003) Accurate First Principles Prediction of ^{17}O NMR Parameters in SiO_2: Assignment of the Zeolite Ferrierite Spectrum. *American Chemical Society*, 125, 541-548.

Profeta, M., Benoit, M., Mauri, F., and Pickard, C.J. (2004) First-principles calculation of the ^{17}O NMR parameters in Ca oxide and Ca aluminosilicates: the partially covalent nature of the Ca-O bond, a challenge for Density Functional Theory. *Journal of the American Chemical Society*, 126, 12628-12635.

Putirka, K.D. (2008) Thermometers and barometers for volcanic systems. In: Putirka, K.D., Tepley, F. (Eds.), Minerals, Inclusions, and Volcanic Processes: *Reviews in Mineralogy and Geochemistry*, 69, 61–120.

Putirka, K., Johnson, M., Kinzler, R., Longhi, J., and Walker, D. (1996) Thermobarometry of mafic igneous rocks based on clinopyroxene-liquid equilibria, 0-30 kbar. *Contributions to Mineralogy and Petrology*, 123, 92-108.

Robinson, K., Gibbs, G.V., and Ribbe, P.H. (1971) Quadratic elongation, a quantitative measure of distortion in coordination polyhedra. *Science*, 172, 567-570.

Rocha, J. (1998) Direct observation of highly distorted hexa-coordinated aluminium in andalusite by very fast ^{27}Al MAS NMR. *Chemical Communications*, 1998, 2489–2490.

Rocha, J., Morais, C.M., and Fernandez, C. (2005) Progress in Multiple-Quantum Magic-Angle Spinning NMR Spectroscopy. *Topics in Current Chemistry*, 246: 141-194.

Sani, A., Delmotte, L., Marichal, C., Gabelica, Z., and Forte, C. (2001) Si-29, Al-27 and Na-23 MAS NMR study of the natural zeolite barrerite and its dehydrated phases. *European Journal of Mineralogy*, 13, 101-111.

Stebbins, J.F. (1987) Aluminum Avoidance Avoided. *Nature*, 330, 13-14.

Stebbins, J.F. (1995) Nuclear Magnetic Resonance Spectroscopy of Silicates and Oxides in Geochemistry and Geophysics. In *Mineral Physics and Crystallography: A Handbook of Physical Constants.* (Table 7 p. 317) AGU Reference Shelf 2. p 303-331. *American Geophysical Union*.

Thompson, P., Cox, D.E., and Hastings, J.B. (1987) Rietveld refinement of Debye-Scherrer synchrotron X-ray data from Al_2O_3. Journal of Applied Crystallography, 20, 79–83.

Warren, M.C., Dove, M.T., Myers, E.R., Bosenick, A., and Palin, E.J. (2001) Monte Carlo methods for the cation ordering in minerals. *Mineralogical Magazine*, 65, 221-248.

Wood, B.J. and Holloway, J.R. (1984) A thermodynamic model for subsolidus equilibria in the system CaO-MgO-Al_2O_3-SiO_2. *Geochimica et Cosmochimica Acta*, 48, 159-176.

Xue, X., and Kanzaki, M. (2008) Structure of hydrous aluminosilicate glasses along the diopside-anorthite join: A comprehensive one- and two- dimensional ^{1}H and ^{27}Al NMR study. *Geochimica et Cosmchimica Acta*, 72, 2331-2348.

Yates, J. R., Pickard, C. J., and Mauri, F. (2007) Calculation of NMR Chemical Shifts for extended systems using Ultrasoft Pseudopotentials. *Physical Review B76*, 024401.

Yoshino, T., Yamamoto, H., Okudaira, T., and Torium, M. (1998) Crustal thickening of the lower crust of the Kohistan arc (N. Pakistan) deduced from Al zoning in clinopyroxene and plagioclase. *Journal of Metamorphic Geology*, 16, 729-748.

FIGURE CAPTIONS:

Figure 1. The crystal structure of CaTs, with stoichiometry $Ca[Al](AlSi)_2O_6$, where [ ] and ( ) indicate octahedral and tetrahedral sites, respectively). The four tetrahedral chains adjacent to M1 are labeled TA, TB, TC and TD according to conventional pyroxene nomenclature. The oxygens at the corners of the tetrahedral are labeled O1, O2 and O3. The structure is drawn using ATOMS by Eric Dowty (www.shapesoftware.com).

Figure 2. ^{27}Al MAS NMR spectra of CaTs. a) 156.2 MHz (14.1 T), b) 234.5 MHz (21.1 T). Inverted triangles indicate spinning sidebands. * indicates corundum.

Figure 3. Two dimensional ^{27}Al 3QMAS NMR spectrum of CaTs at 234.5 MHz (21.1 T). Individual F1 slices have been labeled *a* - *e*. * indicates corundum. Top axis shows MAS NMR projection (F2); Vertical axis shows 3Q projection in the indirect dimension (F1). See text for discussion.

Figure 4. One dimensional slices through peaks *a* – *e* at locations shown in Fig. 3. a) Slice 556: Octahedral peak *a* is surrounded by 2 Al + 4 Si tetrahedral cations. b) Slice 549: Octahedral peaks *b* and *b'*. Peak *b* is surrounded by 3 Al + 3 Si tetrahedral cations. Peak *b'* exhibits significant broadening and quadrupolar lineshape. c) Slice 540: Octahedral peaks *c* and *c'*. Peak *c* is surrounded by 4 Al + 2 Si tetrahedral cations. Peak *c'* exhibits significant broadening and quadrupolar lineshape. d) Slice 459: Tetrahedral peak *d*. This peak is disordered but not distorted. e) Slice 436: Tetrahedral peak *e*

exhibits a quadrupolar lineshape attributed to site distortion. The somewhat distorted line shape for peak *e* (as compared to the fitted peak shape) is often seen for cases with large C_Q. Note: line colors are: data = blue; single peak fit = grey; multiple peak fits = purple and green; sum of multiple fits = red. See Table 4 for DMFIT fit parameters.

Figure 5. Suggested cation arrangements around M1 in CaTs, assuming complete ordering on the tetrahedral chain. a) Structure showing each M1 is surrounded by six corner-sharing tetrahedral cations (two each from TA and TB and one each from TC and TD) and two edge-sharing M1 cations. The octahedral site is occupied by Al (green); The M2 site is omitted for clarity. b-d) The tetrahedral chains are ordered into alternating Al and Si (green and yellow polyhedra, respectively). Changing the relative positioning of the tetrahedral chains produces three unique ordered environments around M1: b) 3 Al + 3 Si, c) 2 Al + 4 Si, and d) 4 Al + 2 Si.

TABLE 1. Crystal structure refinement of CaTs pyroxene RM010K.

Sample	**RM010K**			
P (kb)	20			
T (°C)	1400			
Time (h)	24			
Refinement	Capillary UWO			
Profile type	PV-TCHZ			
Scale	0.0003937 (23)			
displacement	0.0764 (19)			
a (Å)	9.61464 (29)			
b (Å)	8.65470 (26)			
c (Å)	5.27611 (15)			
β (°)	106.0801 (18)			
V (Å^3)	421.858 (22)			
Space Group	C2/c			
Atomic positions	x	y	z	B
T (Si^{4+}) occup. 0.5	0.28740 (26)	0.09783 (32)	0.21376 (46)	0.255 (57)
T (Al^{3+}) occup. 0.5	0.28740 (26)	0.09783 (32)	0.21376 (46)	0.255 (57)
M1 (Al^{3+}) occup. 1.0	0	0.90962 (44)	¼	0.023 (81)
M2 (Ca^{2+}) occup. 1.0	0	0.31084 (27)	¼	0.584 (72)
O1 (O^{2-}) occup. 1.0	0.10448 (43)	0.08222 (56)	0.12474 (83)	0.15 (12)
O2 (O^{2-}) occup. 1.0	0.36434 (43)	0.26782 (53)	0.31118 (90)	0.18 (13)
O3 (O^{2-}) occup. 1.0	0.35279 (46)	0.01978 (45)	0.9777 (11)	0.37 (12)
Crystallite size (nm)	147 (10)			
Strain	0.013 (52)			
Linear Absorption Coeff. (1/cm)	195.644 (10)			
Density (g/cm^3)	3.43434 (18)			
Preferred Orientation (110)	0.9901 (30)			
Profile parameters:				
U	0.071 (10)			
V	-0.076 (11)			
W	0.0188 (27)			
Z	0			
X	0.132 (48)			
Y	0			
Fit Statistics:				
Rbragg	2.558			
Rp	6.77			
Rwp	8.69			
X^2	1.17			
Extra phases (%)	Quartz: 1.5(3) %			

NOTES: The Rietveld method minimizes the residual $R = K \Sigma w_i|y_{i(o)}-y_{i(c)}|^2$, where $y_{i(o)}$ and $y_{i(c)}$ are the observed and calculated intensities, respectively, for each data point (i), $K=1/\Sigma w_i|y_{i(o)}$, $w_i = 1/\sigma(y_{i(o)})^2$, and $\sigma(y_{i(o)})^2$ is the error in $y_{i(o)}$.

* PV-TCHZ = Thompson-Cox-Hastings pseudo Voigt profile function (Thompson *et al*. 1987):

–

** Pref = Preferred orientation: March-Dollase function was used for CaTs with orientation vector [110].

$R_{Bragg} = |I_{n(o)} – I_{(n)c}| / \Sigma I_{n(o)}$ R-Bragg factor

$R_{wp} = \{\Sigma w_i (y_{i(o)}-y_{i(c)}) / \Sigma w_i y_{i(o)}^2\}^2$ R-weighted pattern factor

$R_{exp}= [(N-P)/ w_i y_{i(o)}]^2$ R-expected factor

$\chi = R_{wp}/R_{exp}$ Goodness of fit

where I_n is intensity assigned to the n^{th} Bragg reflection; w is weighting function: $w_i=1/y_i$.

N is the number of data points, I, in the experimental powder profile.

P is the number of parameters refined.

Pro file: RM010K_5bkg_glassfullref_quartzUVWXasCaTs_O-2wErrors2.pro
Data file: RM010K_exp.RAW

TABLE 2. Bond lengths in CaTs.

	CaTs RM010K This study	**CaTs Okamura et al. (1974)**
a (Å)	9.6146(3)	9.6151
b (Å)	8.6547(3)	8.6582
c (Å)	5.2761(2)	5.276
β (°)	106.080(2)	106.12
V ($Å^3$)	421.86(2)	421.94
Bond lengths (Å):		
M1-O1A1, B1	2.011(5)	2.021(1)
-O1A2, B2	1.955(4)	1.947(1)
-O2C1, D1	1.883(5)	1.872(1)
Mean	1.950	1.947
M2-O1A1, O1B1	2.393(5)	2.403(1)
-O2C2, O2D2	2.419(4)	2.420(1)
-O3C1, O3D1	2.492(4)	2.469(1)
-O3C2, O3D2	2.557(5)	2.549(1)
Mean of 6	2.435	2.431
Mean of 8	2.465	2.461
T-O1	1.695(5)	1.693(1)
T-O2	1.663(5)	1.665(1)
Mean non-bridging	1.679	1.679
T-O3A1	1.685(6)	1.683(1)
T-O3A2	1.698(5)	1.701(1)
Mean bridging	1.692	1.692
Overall mean	1.685	1.686

TABLE 3: Polyhedron size and distortion (Quadratic Elongation) for CaTs.

Sample	CaTs RM-010K	Okamura et al. (1974)
	Tetrahedral site:	
Polyhedral Volume ($Å^3$)	2.43	2.4250
Quadratic Elongation (Q.E.)	1.0085	1.0089
Angle Variance (°)	34.3	35.842
	M1:	
Polyhedral Volume ($Å^3$)	9.68	9.6400
Quadratic Elongation (Q.E.)	1.0147	1.0144
Angle Variance (°)	46.1	44.321
	M2:	
Polyhedral Volume ($Å^3$)	24.74	24.5207

Notes: Quadratic Elongation QE $=\lambda = \Sigma [(l_i/l_o)^2/n]$ where l_o = bond length in a regular polyhedron. Angle Variance AV $=\sigma^2 = \Sigma (\theta_i - \theta_o)^2 /n-1)]$ where θ_o is the ideal bond angle and n = coordination number of central atom (both are from Robinson et al. 1971).

Table 4. Measured and fitted parameters from ^{27}Al 3QMAS NMR spectrum of CaTs.

Slice Label*	Reference Spectrum	δ_{F1} (ppm±0.1)	δ_{iso} (ppm±0.2)	C_Q (MHz±0.1)	η_Q (±0.1)	QIS (ppm)	SOQE (MHz)
a	R556	3.0	2.7	5.0	0.5	-3.0	5.2
b	R549	7.5	8.6	4.6	0.7	-2.7	4.9
b′			9.5	9.1	0.6	-10.1	9.6
c	R540	12.9	13.5	5.6	0.7	-4.0	6.1
c'			6.2	9.1	0.6	-10.1	9.6
d	R459	65.4	66.5	5.4	0.5	-3.4	5.6
e	R436	79.6	79.7	11.8	0.45	-16.1	12.2

* Labels appear on Figure 4 and/or they are referred to in the text.

Table 5. Simulated parameters for ^{27}Al 3QMAS NMR of CaTs using Density Functional Theory (DFT).

(See landscape version as a separate attachment.)

Cation Ordering	AABB	Al sites		2Al+4Si					3Al+3Si					4Al+2Si				
				Sim #	δ_{iso} /ppm	$\|C_Q\|$ /MHz	η_Q	δ_{CG} of F_1 /ppm	Sim #	δ_{iso} /ppm	$\|C_Q\|$ /MHz	η_Q	δ_{CG} of F_1 /ppm	Sim #	δ_{iso} /ppm	$\|C_Q\|$ /MHz	η_Q	δ_{CG} of F_1 /ppm
Al sites on A, B, C and D chains are completely ordered: $(Al)[Al]_3(Si)_2$	SiAlSiAl	Tet	1	1	67.3	10.2	0.49	74.5	7	67.6	9.6	0.54	74.1	13	66.7	9.7	0.53	73.3
			2		67.3	10.2	0.49	74.5		66.9	9.6	0.57	73.5		66.7	9.7	0.53	73.3
			3		-	-	-	-		65.9	10.1	0.52	73.0		66.7	9.7	0.53	73.3
			4		-	-	-	-		-	-	-	-		66.7	9.7	0.53	73.3
		Oct	1		**-1.8**	**5.3**	**0.13**	**0.0**		**1.5**	**7.8**	**0.84**	**6.3**		**4.3**	**8.3**	**0.27**	**8.8**
	AlSiSiAl	Tet	1	2	67.0	9.6	0.57	73.6	8	66.6	9.8	0.6	73.5	14	67.4	9.8	0.58	74.3
			2		67.4	9.9	0.58	74.4		66.6	9.8	0.6	73.5		67.6	9.6	0.54	74.1
			3		-	-	-	-		66.6	9.8	0.6	73.5		65.9	10.1	0.52	73.0
			4		-	-	-	-		-	-	-	-		66.9	9.6	0.57	73.5
		Oct	1		**-0.8**	**4.4**	**0.55**	**0.6**		**3.1**	**8**	**0.8**	**8.1**		**7.4**	**4.8**	**0.55**	**9.0**
	SiAlAlSi	Tet	1	3	66.9	9.6	0.57	73.5	9	67.4	9.5	0.62	73.9	15	67.4	9.8	0.58	74.3
			2		67.4	9.8	0.58	74.3		67.4	9.5	0.62	73.9		65.9	10.1	0.52	73.0
			3		-	-	-	-		67.4	9.5	0.62	73.9		66.9	9.6	0.57	73.5
			4		-	-	-	-		-	-	-	-		67.6	9.6	0.54	74.1
		Oct	1		**-0.7**	**4.4**	**0.56**	**0.7**		**2.9**	**1.7**	**0.63**	**3.1**		**7.4**	**4.8**	**0.55**	**9.0**
	AlSiAlSi	Tet	1	4	66.7	9.7	0.53	73.3	10	67.6	9.6	0.54	74.1	16	67.3	10.2	0.49	74.5
			2		66.7	9.7	0.53	73.3		66.0	10.1	0.52	73.1		67.3	10.2	0.49	74.5
			3		-	-	-	-		67.4	9.9	0.58	74.4		67.3	10.2	0.49	74.5
			4		-	-	-	-		-	-	-	-		67.3	10.2	0.49	74.5
		Oct	1		**1.3**	**9.1**	**0.1**	**6.6**		**5.2**	**7.6**	**0.69**	**9.5**		**10.6**	**5.2**	**0.64**	**12.6**
Al sites on A, B, C and D chains are completely disordered: $(Al)[Al]_3(Al)_2$	AlAlSiSi	Tet	1	5	73.3	3.7	0.98	74.5	11	73	3.9	0.92	74.3	17	74.1	3.9	0.93	75.4
			2		74.1	3.8	0.94	75.3		73	3.9	0.92	74.3		73.3	3.7	1.0	74.5
			3		-	-	-	-		73	3.9	0.92	74.3		*	*	*	*
			4		-	-	-	-		-	-	-	-		*	*	*	*
		Oct	1		**-0.3**	**2.9**	**0.8**	**0.4**		**3.9**	**3**	**0.83**	**4.6**		**7.9**	**4.0**	**0.6**	**9.0**
	SiSiAlAl	Tet	1	6	73.3	3.7	0.99	74.5	12	73.6	4.1	0.89	75.0	18	74.1	3.8	0.97	75.3
			2		74.1	3.9	0.93	75.4		73.6	4.1	0.89	75.0		73.3	3.6	1.0	74.4
			3		-	-	-	-		73.6	4.1	0.89	75.0		*	*	*	*
			4		-	-	-	-		-	-	-	-		*	*	*	*
		Oct	1		**-0.2**	**2.9**	**0.8**	**0.5**		**3.8**	**7.7**	**0.81**	**8.4**		**8.0**	**3.9**	**0.6**	**9.1**

Table 5. Simulated parameters for ^{27}Al 3Q MAS NMR of CaTs using Density Functional Theory (DFT).

NOTES:

1. The isotropic chemical shift was obtained relative to kaolinite: the calculated shielding of 544 ppm was computed using the same conditions, and the experimental shift of 6.2 ppm.
2. In the original CIF file, there are 4 octahedral sites and 8 tetrahedral sites by symmetry operations. Therefore, 2Al+4Si, 3Al+3Si, and 4Al+2Si environments can be created for a selected octahedral site. To keep the charge balanced for chemical shielding calculation in CASTEP, the remaining 2 tetrahedral sites are 2 Al for 2Al+4Si, 1 Al and 1 Si for 3Al+3Si, and 2 Si for 4Al+2Si, although in a real sample, the local environment for an octahedral site may have an unbalanced charge.
3. The results shown here are obtained with geometry optimized structures. (CIF Files for simulated structures are available as supplementary material.)
4. * in the column for 4Al+2Si (either AlAlSiSi or SiSiAlAl) indicates that the Al sites in C and D chains are still completely ordered (therefore, not shown), and are assigned to maintain a balanced charge within the structure for the chemical shielding calculation in CASTEP.

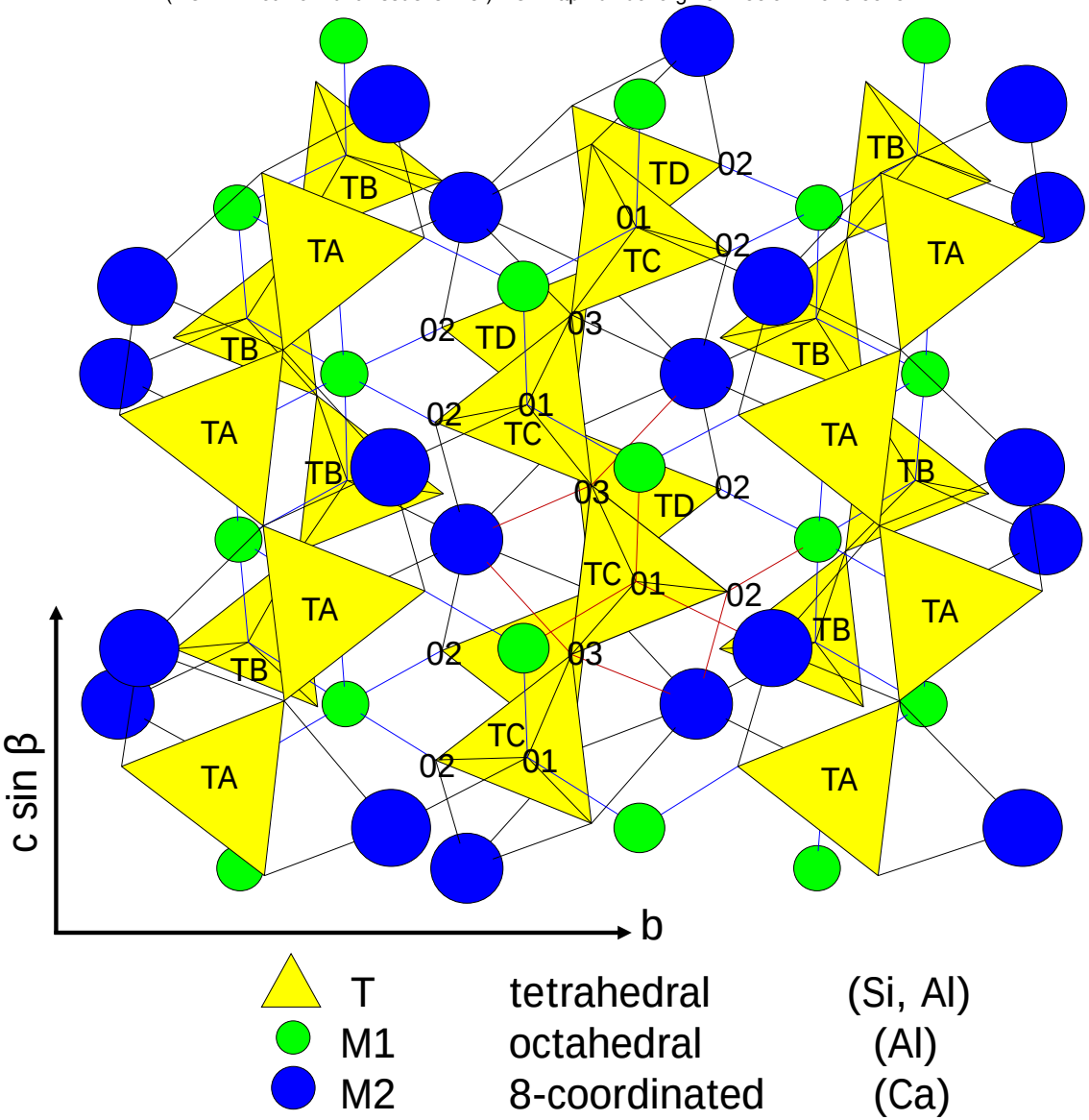

Fig. 1. Flemming et al. (2015)

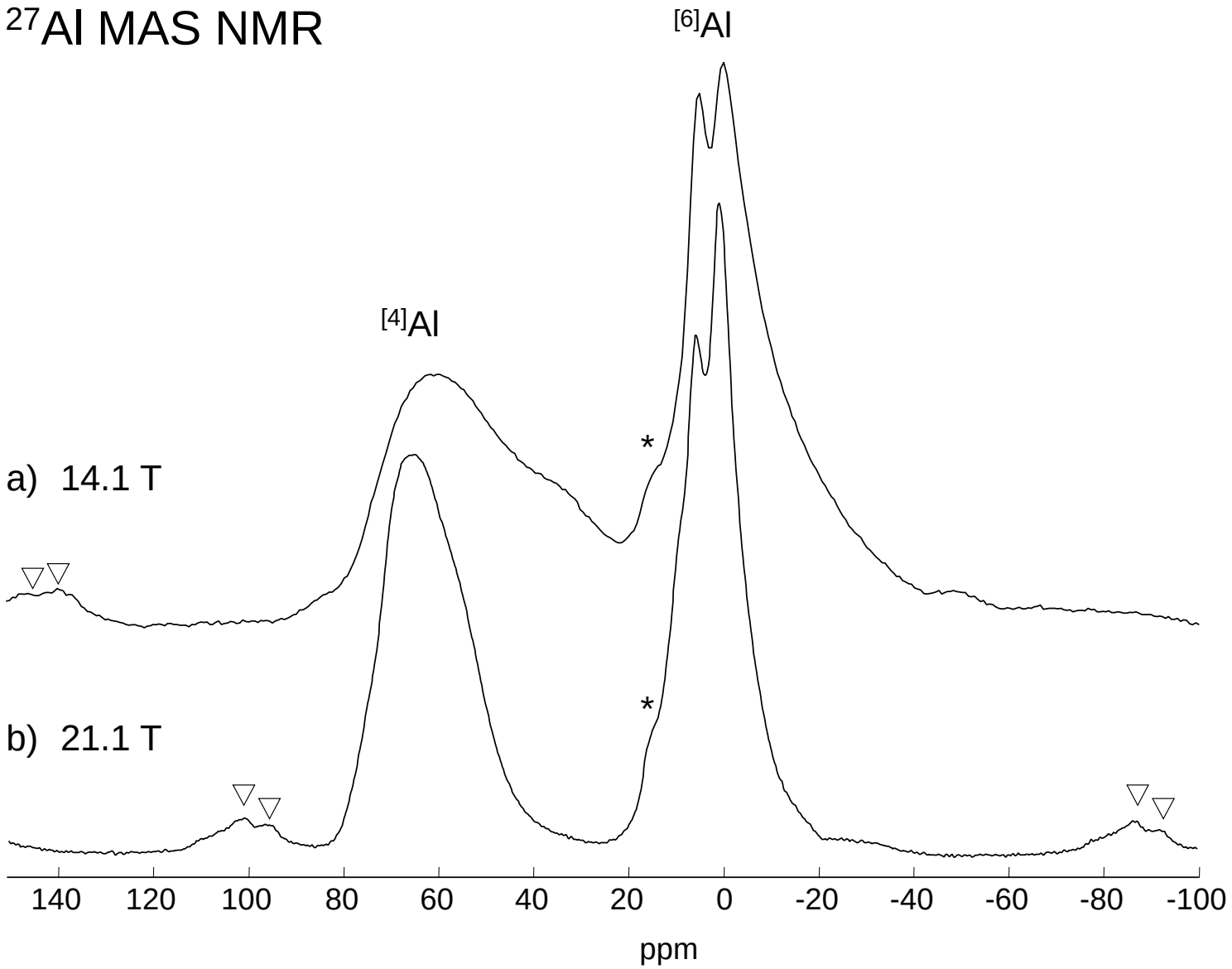

Fig. 2. Flemming et al. (2015)

This is a preprint, the final version is subject to change, of the American Mineralogist (MSA)
Cite as Authors (Year) Title. American Mineralogist, in press.
(DOI will not work until issue is live.) DOI: http://dx.doi.org/10.2138/am-2015-5348

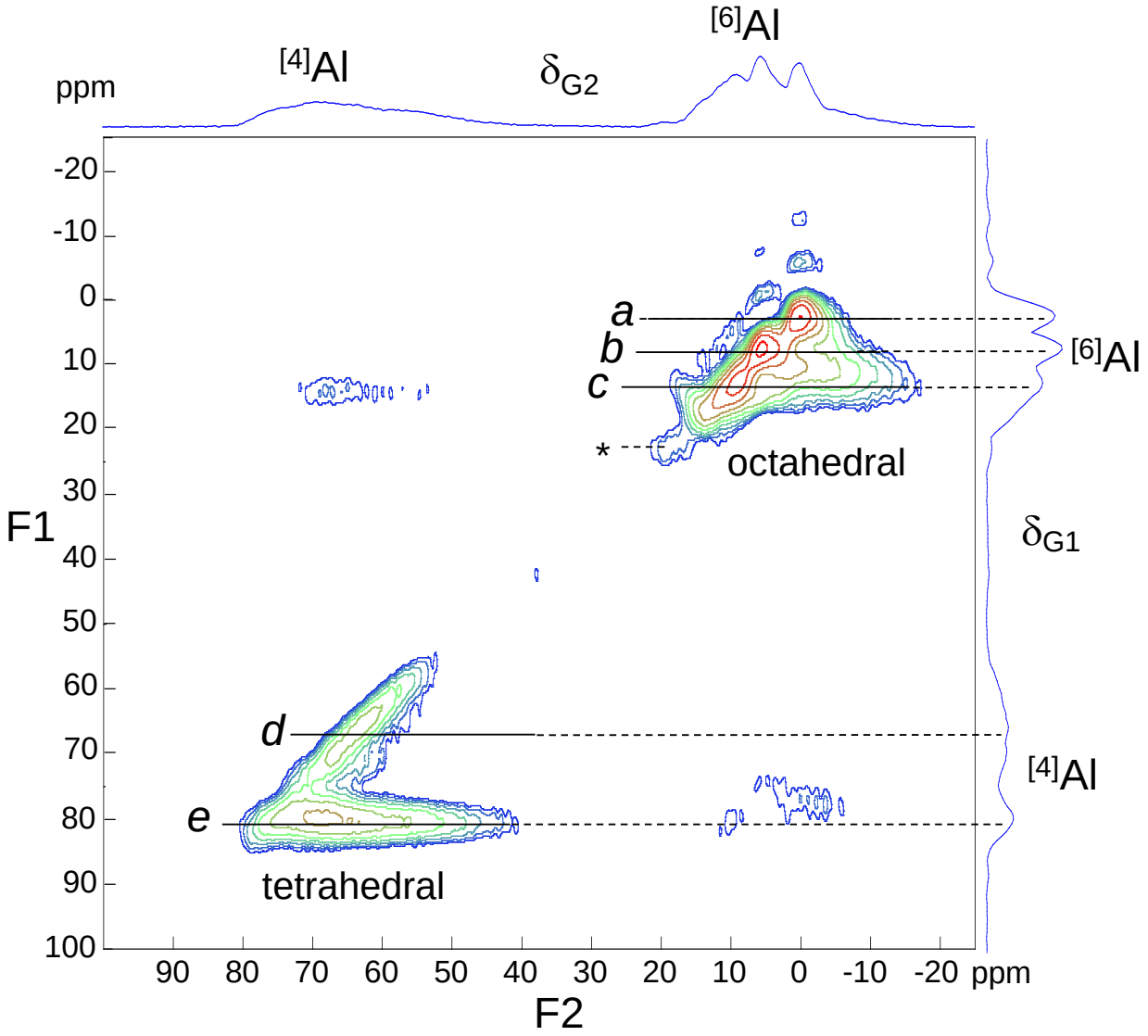

Fig. 3 Flemming et al. (2015)

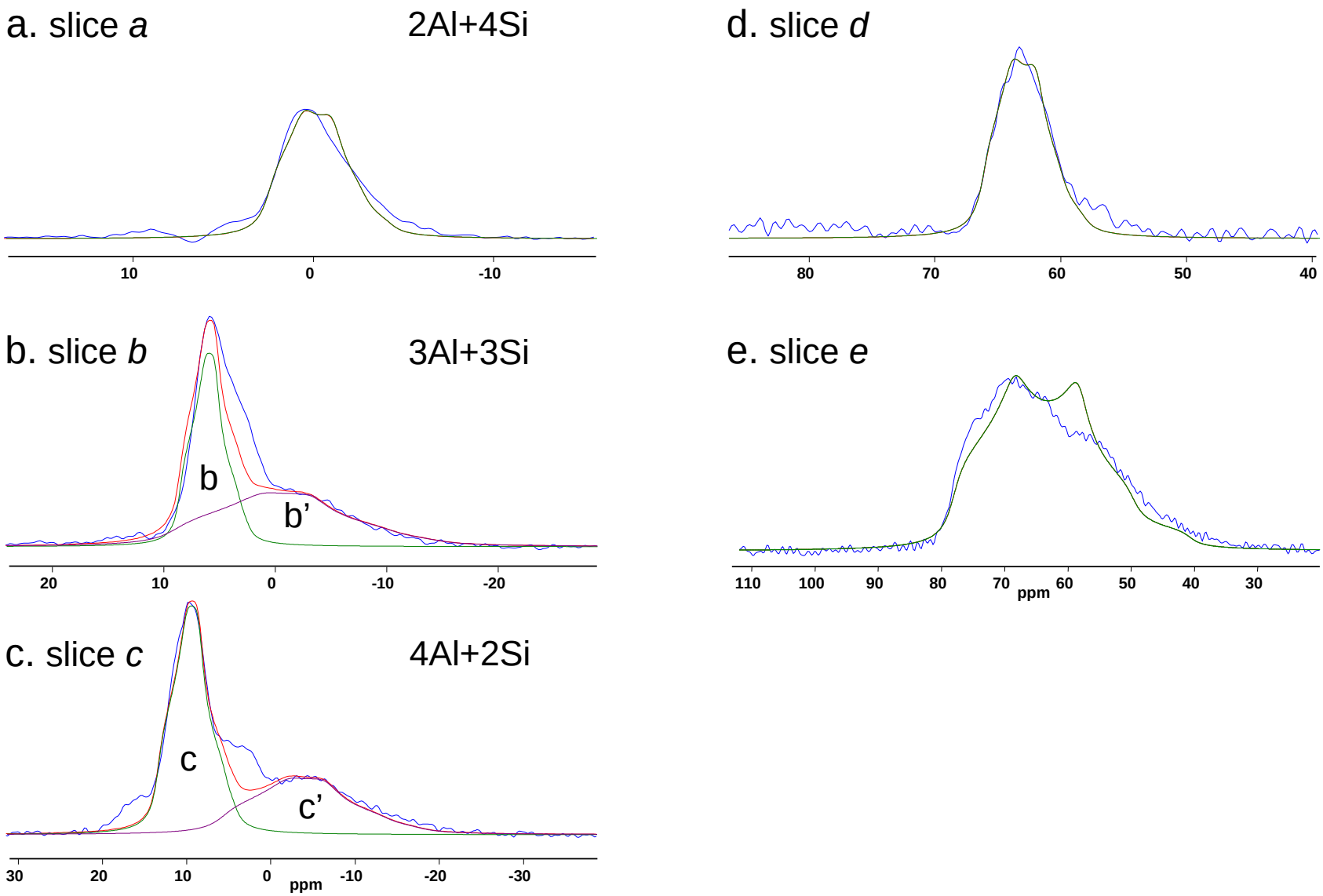

Fig. 4a - e. Flemming et al. (2015)

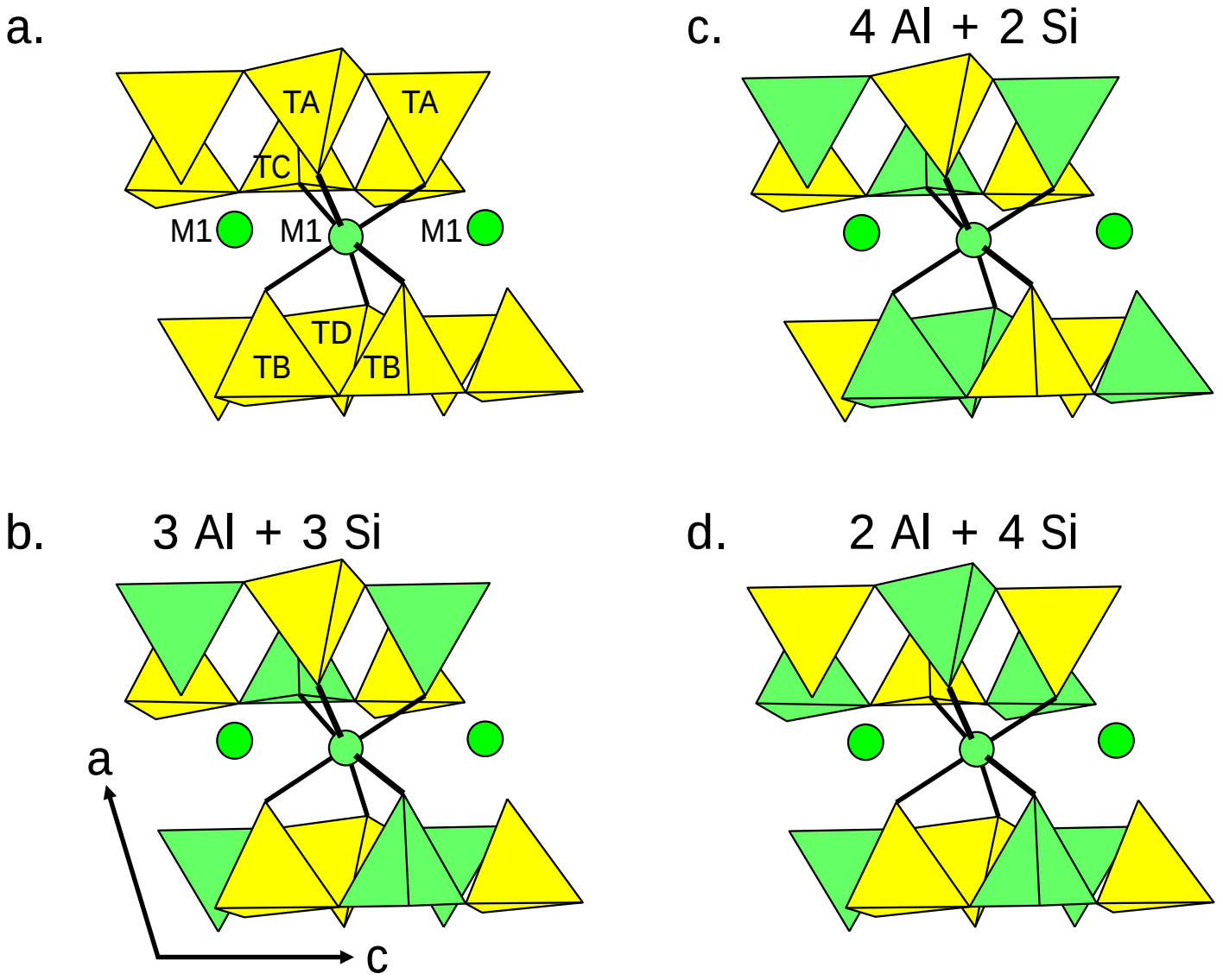

Fig. 5. Flemming et al. (2015)